TAS1R3 is dually required for GTPase signaling in human islet β-cells and skeletal muscle cells

Rajakrishnan Veluthakal[*], Joseph M. Hoolachan[**], Rekha Balakrishnan[**], Karla E. Merz[#], Miwon Ahn, Eunjin Oh and Debbie C. Thurmond

Department of Molecular & Cellular Endocrinology, Arthur Riggs Diabetes and Metabolism Research Institute of City of Hope, Duarte CA.

** **Contributed equally**

Figures: 7
Tables: 0
Word count: 5073
Supplemental material: Suppl. tables=2, figure 1

[#] Present address: Amgen, Thousand Oaks, CA, USA

[*]Corresponding author

Rajakrishnan Veluthakal, Ph.D
rveluthakal@coh.org

Short title: *TAS1R3 functions in human islets and skeletal muscle*

Background: The taste receptor type 1 member 3 (TAS1R3), a G protein coupled receptor, is required for whole body glucose homeostasis. However, the molecular mechanism of TAS1R3 function in islet β-cells and skeletal muscle to control glucose homeostasis remains unknown.

Objective: We questioned whether activation of endogenous TAS1R3 in human islets or clonal human β-cells or human skeletal muscle cells are necessary for glucose stimulated insulin secretion and insulin stimulated glucose uptake respectively *via* activation of small GTPases.

Methods and Results: We found that pharmacological TAS1R3 inhibition (lactisole) in human islets and a human β-cell line diminished glucose-stimulated insulin secretion, attenuated Src family tyrosine kinase signaling, and small GTPase Cdc42 activation. In human skeletal muscle cell lines, lactisole treatment reduced insulin-stimulated glucose uptake, and impaired small GTPase Rac1-dependent non-canonical insulin signaling. We excluded the requirement for the G protein Gαq/11 in TAS1R3 signaling by using the Gαq/11-specific YM-254890 inhibitor in β-cells and skeletal muscle. Notably, the significant reduction of TAS1R3 mRNA and protein levels in human type 2 diabetes pancreatic islets and skeletal muscle, reductions which could be replicated in otherwise healthy cells exposed to diabetogenic stimuli, indicates that the TAS1R3 deficit may be a consequence of diabetogenic stimuli.

Conclusion: Overall, our results suggest that TAS1R3 plays an essential role in GTPase signaling in islet β-cells and human skeletal muscle cells, adding to the growing list of proteins that play a vital role in multiple tissues as therapeutic targets in type 2 diabetes.

ARTICLE HIGHLIGHTS

- Human type 2 diabetic pancreatic islets and skeletal muscle show reduced TAS1R3 levels (> 50%). Exposure of healthy cells to diabetogenic stimuli simulates this reduction, indicating that diabetogenic stimuli may cause TAS1R3 deficit.
- TAS1R3 plays an important role in GTPase signaling in human islets, islet β-cells and human skeletal muscle myotube cells to control glucose homeostasis.
- TAS1R3 is a putative therapeutic target to remediate islet and skeletal muscle defects associated with type 2 diabetes.

About 98 million US adults have prediabetes (1), which is characterized by fasting hyperglycemia (100-125 mg/dl) or impaired glucose tolerance. Further, 1.5 million US adults annually progress from prediabetes to type 2 diabetes (T2D). The current barriers to preventing prediabetes include unsustainable durable lifestyle interventions (i.e., diet and exercise) and/or inadequate current pharmacological options. Therefore, novel therapies that can prevent and/or reverse prediabetes and T2D are urgently needed.

The erosion of the complex and coordinated system between pancreatic islet β-cells for glucose-stimulated insulin secretion (GSIS) and insulin-stimulated glucose uptake in peripheral tissues (e.g., skeletal muscle, liver and adipose) that facilitate whole body glucose homeostasis leads to prediabetes and T2D (2). Normally, elevated circulating glucose increases the glycolytic flux into β-cells, initiating signaling cascades that ultimately lead to Ca^{2+} influx followed by translocation of insulin-laden vesicles towards the plasma membrane for release of their insulin cargo into the circulation (3). The circulating insulin then binds to insulin receptors on peripheral tissues such as skeletal muscle, fat and liver (4). Skeletal muscle contributes to 80% of peripheral insulin-stimulated glucose uptake; this is facilitated by GLUT4-laden vesicle translocation to the sarcolemma (4). Beta cells and skeletal muscle share proteins, whose conserved molecular activities are vital for both GSIS and insulin-stimulated glucose uptake. Importantly, targeting proteins with conserved molecular activities in both islet β-cells and skeletal muscle (e.g., STX4, PAK1, DOC2B, BMP and TXNIP) in T2D has the therapeutic potential to simultaneously improve insulin release by β-cells and insulin sensitivity of skeletal muscle (5-12).

One conserved molecular activity between β-cells and skeletal muscle involves cytoskeletal remodeling for the trafficking of insulin-laden vesicles and GLUT4-laden vesicles toward the cell surface. In both tissues, actin cytoskeleton remodeling is mediated by small Rho-family GTPases (e.g., Cdc42, Rac1) (13-16). In β-cells, glucose activates the Cdc42 signaling cascade that mobilizes insulin granules to the plasma membrane (16). Further, in skeletal muscle, insulin activates the non-canonical Rac1-GTP signaling pathway that enables GLUT4-vesicle translocation to the sarcolemmal and t-tubule membranes (17, 18).

Trimeric GTPases and small-Rho family GTPases coordinate and cross communicate during signaling cascades (19). However, trimeric GTPases that participate in both Cdc42-mediated GSIS from β-cells, and Rac1-mediated glucose uptake into skeletal muscle, remain to be identified. Toward identifying candidates, the sweet taste receptor type 1 member 3 (TAS1R3) was recently implicated in whole body glucose homeostasis (20). Furthermore, a recent study using classic whole body TAS1R3 knockout mice demonstrated impaired glucose tolerance (20). *In vitro*, TAS1R3 was required for insulin secretion from MIN6 β-cells (21). Moreover, TAS1R3 was also required for GLP-1 production in the intestine (22), and amino acid metabolism in skeletal muscle (23). Nevertheless, it remains to be determined the mechanism(s) by which TAS1R3 communicates with small Rho family GTPases in β-cells and skeletal muscle cells.

In this study, we hypothesized that TAS1R3 plays required roles in both GSIS and insulin-stimulated glucose uptake processes. To test this hypothesis, we used a combination of pharmacological and molecular approaches in human donor islets, human

clonal β-cells, human donor skeletal muscles, and clonal LHCN-M2 human myotube cell lines. We demonstrated that TAS1R3 is required for both GSIS and insulin-stimulated glucose uptake utilizing the small Rho family GTPases Cdc42 and Rac1 respectievely. Furthermore, T2D human islets and skeletal muscle biopsies showed deficient levels of TAS1R3 mRNA and protein, suggesting that TAS1R3 deficiency may be a consequence of diabetogenic stress.

Research Design and Methods

Human islets and skeletal muscle

Cadaveric non-diabetic and T2D islets were obtained from the Integrated Islet Distribution Program (IIDP) and from the City of Hope Islet Core (see Supplemental Table S1). Upon arrival, human islets were allowed to recover for 2 h in Connaught Medical Research Laboratories-1066 (CMRL-1066; Thermo Fisher, Waltham, MA), 0.61 g niacinamide, 500 µl ITS Premix Universal Culture Supplement (Thermo Fisher, Waltham, MA), 835 µl Zn_2SO_4 (10 mM stock), 25 ml sodium pyruvate (100 mM stock), 5 ml Glutamax (Thermo Fisher, Waltham, MA), 12.5 ml HEPES (1 M stock), 10% FBS, 5.6 mM glucose, 100 IU/ml penicillin, and 0.1 g/l streptomycin., and then islets were handpicked under a dissecting microscope to yield a purity of >95%.

Cadaveric non-diabetic and T2D skeletal leg muscles were purchased from the National Disease Research Interchange (NDRI, Philadelphia, PA). See Supplemental Table 2 for donor information. The samples were snap-frozen and kept at -80°C until mRNA and protein extraction were carried out.

Human and rat β-cell Culture

EndoC-βH5 and EndoC-βH1 clonal human β-cells were purchased from Human Cell Design (Toulouse, France) and were cultured and used for assays as described in the product manual. INS-1 832/13 cells, gifted from Dr. Christopher Newgard (Duke University Medical Center, Durham, NC) were cultured described previously (24); passage # 52–68 were used.

Quantitative PCR

Total RNA was isolated from human donor samples or INS-1 832/13 cells using the TriReagent according to the manufacturer's protocol (Millipore Sigma, St. Louis, MO, USA)

and assessed using two step reverse transcription (iScript™ cDNA Synthesis Kit, Bio-Rad, Hercules, CA) and qPCR (iQ SYBR® Green Supermix, Bio-Rad, Hercules, CA). Primers used are in Supplemental Table 3. The cycle threshold data was converted to change-fold in expression by the "ΔΔCt" method.

TAS1R3 and Gαq/11 inhibition

Human islets, EndoC-βH1, EndoC-βH5, and LHCN-M2 myotubes cells were exposed to 1 mM lactisole that binds to the transmembrane domain of TAS1R3 and requires 4 key residues for lactisole's sensitivity (25) (Cayman Chemical Company, Ann Arbor, MI) for TAS1R3 antagonism, or 10 μM YM-25490 (Wako Chemicals, Richmond, VA) for Gαq/11 specific antagonism or 0.1% v/v DMSO (vehicle control), by preventing its conversion to its active GTP bound conformation (26). Under certain circumstances, INS-1 832/13 cells were exposed to fenofibrate (10 μM or 27.17 μM; Cayman Chemical Company, Ann Arbor, MI) for TAS1R3 inhibition for 20 min.

Static incubation assay for GSIS

Human islets were incubated for 2 h at 37 °C in Krebs-Ringer bicarbonate buffer (KRBH) as described previously (13). For TAS1R3 or Gαq/11 inhibitor studies islets were exposed for 20 min (as above), followed by 1 h stimulation with either 1 mM (low glucose) or 20 mM glucose (high glucose). Secreted insulin was measured using an ELISA kit for human insulin (Mercodia, Winston Salem, NC). Insulin content from donor islets solubilized in Nonidet P-40 lysis buffer was quantified by ELISA relative to total islet protein for each batch of human islets using DC Protein Assay kit (Bio-Rad, Hercules, CA).

EndoC-βH5 cells were seeded onto βCoat® coated 96-well plates. Six days later, medium was replaced with Ulti-ST® starvation medium containing 0.5 mM glucose for 24

h. Medium was then replaced with βKrebs® GSIS buffer supplemented with 0.1% fraction V fatty acid free BSA for 40 min, followed by addition of TAS1R3 or Gαq/11 inhibitor for 20 min. Cells were then incubated with βKrebs®/BSA supplemented with high glucose (16.7 mM) for 45 min. Incubation medium was collected, spun down and analysed by ELISA. For insulin content, cells were lysed in Tris/Triton X-100 based lysis buffer for 5 min, collected and analysed by ELISA. Insulin was measured by ELISA using Human Insulin Kit (Mercodia, Winston Salem, NC) following manufacturer's instructions.

Glucolipotoxicity Exposure

INS-1 832/13 cells were grown in INS-1 medium as described previously (24) until 80% confluent and then cultured in INS-1 medium containing 25 mM glucose and 0.4 mM palmitate (27) for various time periods, as indicated in the figure legends.

Small Interfering RNA Transfection

siRNA against TAS1R3 and control non-targeting siRNA duplexes were purchased from OriGene (Rockville, MD). siRNA oligonucleotides were transfected into INS-1 832/13 cells using Lipofectamine™ RNAiMAX transfection reagent (Thermo Fisher, Waltham, MA) and opti-MEM (Thermo Fisher, Waltham, MA) at 1.0, 10 and 50 nM. Post-36 h transfection, INS-1 832/13 cells were equilibrated in 2.5 mM glucose and 2.5% serum culture medium overnight, followed by a 1 h exposure to glucose-free KRBH. Secreted insulin during GSIS was assayed as above. Post-GSIS assay, cells were harvested in 1% NP-40 lysis buffer to determine TAS1R3 knock-down efficacy by immunoblot.

Immunoblot analysis

Rabbit polyclonal TAS1R3 (1:1000, Thermo Fisher Scientific, Waltham, MA) were used to detect the abundance of TAS1R3 from skeletal muscle, human islets and EndoC-

βH1. For active phospho-SFK (Tyr^{416}), 1:1000 rabbit polyclonal antibody (Thermo Fisher Scientific, Waltham, MA) was used. As a control for equivalent protein-loading in individual wells of the polyacrylamide gel, the content of t-SFK was detected using a rabbit monoclonal antibody (1:1,000, Cell Signaling Technology, Danvers, MA). Goat anti-rabbit (1:10,000, Bio-Rad, Hercules, CA) or goat anti-mouse (1:20,000, Bio-Rad, Hercules, CA) HRP-conjugated secondary antibodies were used for enhanced chemiluminescence detection (ECL, GE Healthcare, Chicago, IL).

For the detection of membrane-bound TAS1R3, rabbit polyclonal TAS1R3 (as above), was used. As a control for equivalent protein-loading in individual wells of the polyacrylamide gel, the content of STX4 was detected using mouse monoclonal STX4 (1:5,000, BD Transduction Laboratories, San Diego, CA). HRP-conjugated secondary antibodies were used for ECL detection (as above). Mouse monoclonal Rho-GDIα antibody (1:5,000, Santa Cruz Biotechnology, Inc., Dallas, TX), a cytosolic marker was used to measure the purity of plasma membrane fractions, and whole cell lysates were used as a positive control.

For detection of insulin signaling pathway IRS (Tyr^{608}, 1: 1,000, Millipore-Sigma, St. Louis, MO), AKT (Ser^{473}, 1:1,000, Cell Signaling Technology, Danvers, MA) (28) and cofilin (Ser^{3}, 1:1,000, Santa Cruz Biotechnology, Inc. Dallas, TX) (29) were used. As a control for equivalent protein-loading, IRS (1:1000, Cell Signaling Technology, Danvers, MA), AKT (1:1,000, Cell Signaling Technology, Danvers, MA) and Cofillin (1:1,000, Cell Signaling Technology, Danvers, MA) and GAPDH (1;50, 000, Invitrogen, Waltham, MA) antibodies were used.

Cdc42 and p-SFK(Tyr^{416}) activation assay

Human islets or EndoC-βH1 cells were equilibrated in low glucose (2.5 mM) and low serum (2.5%) culture medium overnight, followed by a 1 h exposure to glucose-free KRBH. Cells were exposed to KRBH containing antagonists (as above), after which the experiment was conducted for 1 min (Phosphorylation-SFK activation) and 2 min (Cdc42 activation) using fresh test solutions with low (2.8 mM) or high (16.7 mM) glucose. After stimulation, cells were harvested in 1% Nonidet P-40 lysis and Phospho-SFK (Tyr^{416}) was determined using immunoblot analysis (see above). G-LISA (Cytoskeleton Inc (Cat # BK 127) was used to quantify the amount of active Cdc42-GTP from human islets and EndoC-βH1 cell lysate as described previously (13).

Intracellular cAMP measurements

EndoC-βH5 were equilibrated in βKrebs® GSIS buffer supplemented with 0.1% fraction V fatty acid free BSA for 40 min, followed by addition of TAS1R3 or Gαq/11 inhibitor for 20 min. Cells were then incubated with βKrebs®/BSA supplemented with glucose (16.7 mM) for 45 min. On day of cAMP assay 1 mM phenylmethylsulfonyl fluoride (PMSF) was added to cell lysates; intracellular cAMP levels were measured using a Direct cAMP ELISA kit from Enzo Life Sciences, Inc. (Farmingdale, NY) as per manufacture's protocol.

Plasma Membrane Isolation

EndoC-βH1 were equilibrated in low glucose (2.8 mM) and low serum (2.5%) culture medium overnight, followed by followed by a 1 h exposure to glucose-free KRBH. Plasma membrane fractions of EndoC-βH1 glucose-stimulated cells (16.7 mM glucose, 15 min). cells were isolated as previously described (30). The proteins were further separated using SDS-PAGE and transferred to the PVDF membrane. Rho-GDIα, a cytosolic marker,

was used to validate the purity of plasma membrane fractions; whole cell detergent clarified lysates served as positive control for antibody detection capability.

LHCN-M2 Myoblast Cell Culture

For physiological relevance of TAS1R3 knockdown in skeletal muscle, the immortalized human LHCN-M2 skeletal myoblast cell line was used (a generous gift from Dr. Melissa Bowerman, Keele University, UK). LHCN-M2 myoblasts were cultured in complete growth medium (4:1 ratio of 5 mM glucose DMEM (Thermo Fisher, Waltham, MA) and 5 mM glucose M199 medium (Thermo Fisher, Waltham, MA) supplemented with 15% [v/v] HI-FBS, 1% [v/v] antibiotic-antimycotic solution, 20 mM pH 7.4 HEPES buffer, 30 ng/mL Zn_2SO_4, 1.4 μg/mL vitamin B12 (Sigma-Aldrich, St. Louis, MO), 55 ng/mL dexamethasone (Sigma-Aldrich, St. Louis, MO), 2.5 ng/mL recombinant human hepatocyte growth factor (Sigma-Aldrich, St. Louis, MO), and 10 ng/mL recombinant human basic FGF (Biopioneer, San Diego, CA) on plastic cell culture dishes pre-coated with 1% [w/v] autoclaved porcine gelatin (Sigma-Aldrich, St. Louis, MO). At >70% confluence, LHCN-M2 myoblasts were cultured in complete differentiation medium composed of DMEM/M199 4:1, 2% [v/v] heat-inactivated horse serum (HI-HS) (Thermo Fisher, Waltham, MA), 1% [v/v] anti-biotic/anti-mycotic solution, 20 mM pH 7.4 HEPES buffer, 30 ng/mL Zn_2SO_4, and 1.4 μg/mL vitamin B12 for 6 days with fresh media changes every 48 h in 37°C and 5% CO_2 incubator until multi-nucleated myotubes formed. For GLT-induced diabetogenic stress, LHCN-M2 myotubes were exposed to 200 μM palmitate and 25 mM glucose for 16 h.

LHCN-M2 2-Deoxyglucose uptake

LHCN-M2 myotubes were transfected with either siRNA against TAS1R3 and control non-targeting siRNA duplexes using Lipofectamine™ RNAiMAX transfection reagent (Thermo Fisher, Waltham, MA) for 6 hours, before fresh media change for an additional 42 h. For 2-Dexoyglucose uptake the myotubes underwent 2x PBS wash and were then serum- and glucose-starved in oxygenated FCB buffer for 2 h, concurrently the myotubes were either unstimulated (basal) or insulin stimulated at 100 nM for 20 min followed by the 2-DG protocol described for L6.GLUT4myc myotubes (31).

G-LISA for Rac1 activation assay

Rac1 activation was measured in the cell lysate from LHCN-M2 myotubes using the commercially available G-LISA Rac1 Activation Assay from Cytoskeleton Inc (Denver, CO) (13). Briefly, LHCN-M2 myotubes underwent 2x PBS wash and were then serum-starved serum- and glucose-starved in oxygenated FCB buffer for 1 h. Concurrently, the myotubes underwent 1 h treatment with either DMSO control (0.1% v/v), 1 mM lactisole or 10 μM YM-254890 to induce TAS1R3 (lactisole) or Gαq/11 (YM-254890) pharmacological inhibition before 10 minutes of 100 nM insulin stimulation against basal controls. Rac1 activation was measured in the supernatant using the commercially available G-LISA Rac1 Activation Assay from Cytoskeleton Inc (Cat # BK 128) (32). Intensity of the color formed from the chromogenic substrate was quantified by colorimetry using a BioTek Synergy HTX Multi-Mode Plate Reader.

Statistics

Data are presented as mean ± SEM and *n* values are indicated in the figures. Differences between two groups were assessed using Student's t-test. Statistically significant differences among multiple groups were evaluated using one-way or two-way ANOVA followed by Bonferroni post hoc test. The threshold for statistical significance was set at $p < 0.05$ and all analyzed using GraphPad Prism software, version 8.3.0. Statistical significance is indicated in the figure legends.

Data and Resource Availability

The data sets generated during and/or analyzed during the current study are available from the corresponding author upon reasonable request. No applicable resources were generated during this study.

RESULTS

TAS1R3 mRNA and protein levels are reduced in T2D human islets

TAS1R3 abundance was significantly reduced in type 2 diabetic islets compared to non-diabetic controls (**Fig. 1A-B**). Further, a time-dependent reduction in TAS1R3 was confirmed in rat clonal β-cells (INS-1 832/13) exposed for 16 or 24 h to diabetogenic glucolipotoxic (GLT: 25 mM glucose, 400 μM palmitic acid) stress (**Fig. 1C-D**). The concentrations of GLT used in the current studies have been validated in INS-1 832/13 clonal β-cells (27, 33). Given that endoplasmic reticulum (ER) stress is a hallmark feature of GLT-induced β-cell dysfunction, we measured CHOP. CHOP levels were significantly elevated within 24 h of GLT exposure (**Fig. 1C**). This suggests that the reduction in β-cell TAS1R3 levels may result from glucolipotoxic diabetogenic stress in T2D human islets.

Inhibition of TAS1R3, and its potential downstream G-protein target Gαq/11, impairs GSIS, but only TAS1R3 is required for cAMP.

TAS1R3 is known to interact with multiple G-protein subfamilies (34, 35). Indeed, β-cell specific Gαq and Gα11 double knockout (KO) mice displayed glucose intolerance linked to impaired insulin secretion capacity (36). Thus, we questioned whether TAS1R3 plays a role in pancreatic β-cell insulin secretion, and whether this involved coupling to Gαq/11. We assessed GSIS inhibition in human islets (**Fig. 2A**) and human EndoC-βH5cells (**Fig. 2B**) following selective inhibition of Gαq/11 (YM-254890, Gαq/11*i*) or TAS1R3 (lactisole, TAS1R3*i*): both inhibitors significantly reduced GSIS compared to the vehicle control. The TAS1R3*i* exhibited a dose-dependent inhibition in the human

EndoC-βH5 cells (Fig. 2B, bar 8 vs. bar 6), therefore the higher dose (1 mM) was used for all subsequent studies. Treatment regimens involving Gαq/11*i* and TAS1R3*i* were without impact upon insulin content (**Supplemental Fig. 1**). Cyclic adenosine monophosphate (cAMP) is a downstream mediator of GSIS, *via* small GTPase activation (13). Therefore, we measured cAMP levels post-Gαq/11 or -TAS1R3 inhibition in human EndoC-βH5 cells. As expected stimulatory glucose evoked a significant increase in cAMP levels in vehicle treated cells; on the other hand, cAMP levels were only reduced post-TAS1R3 inhibition, while Gαq/11 inhibition was without effect (**Fig. 2C**). Additionally, we tested another inverse agonist of TAS1R3, fenofibrate, a drug commonly used to lower cholesterol in T2D patients (37). Indeed, long-term fenofibrate treatment impairs GSIS in obese rats (38). As with the TAS1R3*i*, fenofibrate at a dosage of 10 μM and 27.17 μM significantly inhibited GSIS (**Fig. 2D**). The fenofibrate dosage of 27.17 μM we tested is relevant in humans, since in patients a single dose of 300 mg fenofibrate reaches concentrations of approximately 10 mg/L in plasma, which is 27.17 μM (39).

We further tested the requirement for TAS1R3 in GSIS using siRNA-mediated knockdown. In INS-1 832/13 cells, we observed a concentration dependent knockdown of TAS1R3 (0-50 nM), achieving ~45% knockdown efficiency using 50 nM of TAS1R3-specific-siRNA as compared with control-siRNA at protein level (**Fig. 3A)**. TAS1R3-siRNA dose-dependently inhibited GSIS compared with control siRNA or non-transfected cells (**Fig. 3B**). Overall, both pharmacological inhibition and genetic knockdown of TAS1R3, suggests that it is required for GSIS through cAMP.

Inhibition of TAS1R3 attenuates Src family kinase and Cdc42 activation events required for GSIS

The glucose-stimulated activation of Cdc42 in β-cells requires upstream YES kinase (a Src family kinase, SFK) signaling (40). To date, YES kinase is the only member of the SFK family that responds to high glucose in β-cells, detected using a pan-SFK pTyr416 antibody. Since glucose-stimulated cAMP accumulation enhances Cdc42 activity (13), we questioned if TAS1R3 played a role in SFK-mediated Cdc42 activation. We treated EndoC-βH1 cells with TAS1R3*i* or Gαq/11*i* inhibitor and measured SFK activation, and determined that TAS1R3*i* but not Gαq/11*i* blunted pSFK activation (**Fig. 4A**). We further assessed the effects of these inhibitors upon Cdc42 activation in human islets and human EndoC-βH1 cells. Compared to vehicle control, only TAS1R3 inhibition significantly ablated Cdc42 activation; Gαq/11 inhibition was without effect (**Fig. 4B-C**). Hence, SFK and Cdc42 activation events are TAS1R3-dependent, while the Gαq/11 requirement in GSIS occurs *via* a different pathway.

Following activation, most GPCRs employ the β-arrestin-dependent clathrin-mediated endocytosis pathway for receptor desensitization, internalization and subsequent recycling or degradation (41). As such, we investigated TAS1R3 abundance at the plasma membrane (PM) in human EndoC-βH1 cells after 15 min of stimulatory glucose. Cells were stimulated with high glucose (16.7 mM) or low glucose (2.8 mM) for 15 min, and immediately sub-fractionated to evaluate changes in membrane-associated TAS1R3 abundances. PM-TAS1R3 was significantly diminished post-15 min glucose stimulation, relative to the static plasma membrane protein STX4, compared with

TAS1R3 abundance at the PM in unstimulated (2.8 mM glucose) cells (**Fig. 4D)**. Furthermore, treatment with the TAS1R3 inhibitor Lactisole prevented the high-glucose induced reduction of TAS1R3 abundance at the PM at 15 min post-glucose stimulation. Consistent with other glucose-sensitive functional GPCR in β-cells (42), these findings suggest that TAS1R3 internalizes in response to stimulatory glucose.

TAS1R3 transcript and protein levels are decreased in T2D human skeletal muscle

Skeletal muscle insulin resistance is a major pathological feature in T2D (43). First, we assessed TAS1R3 levels in human LHCN-M2 myotubes exposed for 16 h to diabetogenic glucolipotoxic (GLT: 25 mM glucose, 200 μM palmitic acid) stress, the levels of TAS1R3 mRNA were significantly reduced under the duress of stress (**Fig. 5A).** Thus, we next assessed TAS1R3 levels in patient-derived skeletal muscle biopsies. TAS1R3 mRNA and protein levels were significantly reduced (> 50%) in T2D skeletal muscle compared with that of non-diabetic skeletal muscle (**Fig. 5B-C**). Thus, the reduced TAS1R3 levels observed in T2D skeletal muscle may result from GLT-induced diabetogenic stress and could contribute to the pathological dysregulation in peripheral glucose uptake.

TAS1R3 inhibition impedes insulin-stimulated glucose uptake via a non-canonical insulin signaling pathway

To determine the requirement for TAS1R3 in skeletal muscle peripheral glucose uptake, we evaluated the impact of TAS1R3 or Gαq/11 inhibition against a vehicle control in insulin-stimulated human LHCN-M2 myotubes by measuring [^{3}H]2-DG radioactivity.

TAS1R3 inhibition significantly impeded glucose uptake by ~50% versus the vehicle in insulin-stimulated human LHCN-M2 myotubes (**Fig. 6A**). By contrast, Gαq/11 inhibition failed to impair glucose uptake (**Fig. 6A**), In skeletal muscle, activation of the small GTPase Rac1 is required to mobilize GLUT4-laden vesicles to supply the GLUT4 protein at the sarcolemma to facilitate insulin-stimulated glucose uptake *via* a non-canonical insulin pathway (18). We tested the requirement for TAS1R3 in Rac1 activation in human LHCN-M2 myotubes by inhibiting TAS1R3 and comparing with Gαq/11 inhibition. While neither inhibitor altered basal conditions (**Fig. 6B**), only TAS1R3 inhibition significantly reduced insulin-stimulated Rac1-GTP levels (**Fig. 6B**). To verify that the decrease in insulin-stimulated glucose uptake in skeletal muscle was TAS1R3-specific, our knockdown of TAS1R3 levels *via* siRNA transfection (**Fig. 6C)** significantly reduced insulin-stimulated [^{3}H]2-DG uptake (**Fig. 6D**), indicating a selective role for TAS1R3 in insulin-stimulated glucose uptake into human LHCN-M2 myotubes.

We next investigated the impact of TAS1R3 inhibition on canonical and non-canonical insulin signaling cascades. Canonical insulin-signaling was assessed in LHCN-M2 myotubes, and TAS1R3 inhibition had no significant effect on phosphorylation (activation) of canonical insulin cascade components IRS1 (Tyr^{608}) and AKT (Ser^{473}) (**Fig. 7A-B**). Non-canonical insulin signaling downstream of Rac1 involves Cofilin, a protein that oversees actin remodeling to translocate GLUT4-laden vesicles to the plasma membrane; Cofilin phosphorylation leads to depolymerization of actin filaments, which impedes GLUT4 vesicle translocation in skeletal muscle cells (29, 44). While vehicle control myotubes responded to insulin stimulation with >50% decrease of p-Cofilin

(relative to total cofilin protein), TAS1R3*i*-treated human myotubes failed to show this insulin-stimulated decrease in p-Cofilin (**Fig. 7C**). Similar to our previous results on insulin-stimulated glucose uptake and Rac1 activation in human myotubes (**Fig. 6**), Gαq/11 inhibition had no impact on either canonical and non-canonical insulin signaling components (**Fig. 7A-C**). Although the mechanism of action remains to be determined, our results suggests that TAS1R3 plays an independent role in non-canonical insulin signaling *via* Rac1 activation that supports insulin-stimulated glucose uptake in LHCN-M2 myotube skeletal muscle cells.

DISCUSSION

This study provides novel mechanistic insights into the glucose homeostatic role of TAS1R3-mediated trimeric GTPase signaling events that facilitate GSIS from β-cells, and insulin-stimulated glucose uptake into LHCN-M2 human skeletal muscle cells. There are two SNP's associated with TAS1R3 gene (TAS1R3 rs307355 and rs35744813) and multivariate analysis normalized for age, sex, and BMI, showed previously a significant decrease in sensitivity to sweet stimuli, suggesting TAS1R3 is important for sweet sensing (45). Our data in human T2D islet and skeletal muscle samples displayed significantly reduced TAS1R3 levels compared to non-diabetic controls, consistent with the impaired glucose tolerance and insulin resistance phenotype observed in the TAS1R3 knockout mice (20). Further, we revealed a specific role for TAS1R3 in β-cell non-canonical Cdc42 signaling *via* TAS1R3 depletion and inhibition and in non-canonical Rac1 mediated insulin signaling *via* TAS1R3 inhibition in skeletal muscle cells. Collectively, these studies reveal TAS1R3 could be a new candidate target that may serve dual positive roles in these two pivotal metabolic tissues, with the capacity to orchestrate improved glucose homeostasis.

These findings elucidate the most upstream event, TAS1R3 activation, spearheading each of the non-canonical signaling cascades required for GSIS from β-cells and insulin-stimulated glucose uptake into skeletal muscle. It was unexpected that the same GPCR initiated these cell-type specific processes, given the distinct downstream effectors in each cascade. However, each of these processes involves actin cytoskeleton remodeling to facilitate insulin granule and GLUT4 vesicle trafficking to their respective cell surface membranes (46). TAS1R3 did not to couple to Gαq/11, and instead coupled *via* the Rho

family GTPases — Cdc42 in β-cells and Rac1 in human skeletal muscle cells; each is required for actin remodeling *via*PAK1 activation in their respective cell type (6, 29, 44). However, beyond PAK1, the cascades differ significantly in these cell types. For example, skeletal muscle PAK1 signaling involves p41ARC, N-WASP and Cortactin to build F-actin tracks to shuttle GLUT4 vesicles out to the sarcolemmal and t-tubule membranes (47). In contrast, β-cell PAK1 signaling diverges through Rac1 and Raf/MEK/ERK to culminate in a net decrease in F-actin at the cortical plasma membrane (48, 49). Currently, GPCR ligands/agonists are being pursued in a therapeutic context given the ability to activate them extracellularly and harness their signaling cascades to evoke either insulin secretion or insulin action (glucose uptake). Our work here strongly supports the notion that a single agent that targets a factor that has conserved molecular activities in both islet β-cells and skeletal muscle could simultaneously impact both insulin secretion and peripheral insulin action.

Our use of selective short-duration pharmacologic inhibitors of TAS1R3 activity supports the concept that there is an acute need for TAS1R3 signaling in each cell type and process. Moreover, our GLT results suggested TAS1R3 transcriptional and post-transcriptional downregulation, supporting the concept that exposure to dietary diabetogenic stimuli causes loss of TAS1R3 in β-cells. We further corroborated this reduction in TAS1R3 mRNA and protein levels in human T2D islets. Additionally, we found that fenofibrate inhibited GSIS *in vitro*. Fenofibrate is a commercial drug that mitigates clinical dyslipidemia (50), and is a known TAS1R3 inhibitor (51). Yet in spite of the beneficial effect on plasma lipid levels (plasma triacylglycerol and NEFA), fenofibrate treatment (0.1%; 3 weeks) of mice almost completely abolished the acute phase of insulin secretion, (50). Our findings are consistent with this evidence, and contribute to the

mechanistic understanding of the observed diabetes risk with fenofibrate use.

TAS1R3 activation precedes Src kinase YES activation, revealing the foremost signaling event triggering the signaling cascade linking small GTPases→actin remodeling→GSIS in β-cells. The glucose-stimulated phosphorylation of SFK, particularly of YES kinase, was previously reported to be a key proximal step in the activation of Cdc42 (40), and essential for actin cytoskeletal remodeling. Lactisole inhibition of TAS1R3 blunted glucose-induced activation of phospho-SFK and of Cdc42, suggesting the first known signaling cascade emanating from TAS1R3 signaling in the β-cell. The binding of Gα subunits of trimeric GTPases to the SFK catalytic domain causes conformational changes in SFK family members, leading to increased accessibility of the active site to substrates (52), and in this case, Cdc42. The activation of SFK by trimeric GTPases are specific for Gα and Gαi, but not for Gαq, Gα12 nor Gβy (52). The inability of YM-25490 (an inhibitor of Gαq/11) to impact SFK and subsequent Cdc42 activation in our study is consistent with this concept. Further studies are required to identify the trimeric GTPase cascade that potentially occur concurrently, yet independently of TAS1R3 signaling, to regulate GSIS.

In human skeletal muscle cells, the only previously reported roles for TAS1R3 were related to myogenesis and amino acid sensing to activate mTOR for inhibition of autophagy (23). This study demonstrates a novel role for TAS1R3 in insulin-stimulated glucose uptake *via* the activation of the small GTPase Rac1, in the non-canonical insulin signaling cascade that promotes F-actin remodeling for GLUT4-vesicle translocation that facilitates insulin-stimulated glucose uptake. How TAS1R3 modulates Rac1-GTP activation in this non-canonical insulin signaling pathway remains to be elucidated. The

inability of YM-254890 to emulate lactisole effects in insulin-stimulated human LHCN-M2 myotubes implies that TAS1R3 acts through a G-protein independent of Gαq/11. Given that FR900359, a Gαq/11/14 inhibitor (53) was shown to impede GLUT4 translocation and insulin-stimulated glucose uptake in skeletal muscle cells, $G\alpha_{14}$ may be a putative candidate. Future studies are needed to determine the key G-protein candidate(s) downstream of TAS1R3.

In conclusion, our findings provide novel insights into the functional activity of TAS1R3 in whole body glucose homeostasis. Even though we identified TAS1R3 as a modulator of GSIS and insulin-stimulated glucose uptake *via* small GTPases Cdc42 (β-cells) and Rac1 (skeletal muscle cells), the putative trimeric GTPase(s) other than Gαq/11 that facilitates these events remains to be identified. One potential limitation in the current study is the lack of demonstration of TAS1R3 functional implications in cell type specific conditional knockout animal models in vivo; at present, only classic whole body models exist, and given the importance of TAS1R3 in multiple endocrine cell types that contribute to glucose homeostasis, future studies will require generation of inducible, conditional knockout mouse models. These emerging mechanistic insights facilitate the addition of TAS1R3 to the growing list of factors that play a dual role in multiple tissues as a therapeutic target that remediate islet and skeletal muscle defects associated with T2D.

ARTICLE INFORMATION

Acknowledgements
The authors thank the United Network for Organ Sharing (UNOS) for providing donated pancreata for human islet isolation. We also thank the Integrated Islet Distribution Center (IIDP) and Southern California Islet Cell Resource (SC-ICR) Center at City of Hope, for preparing and providing the majority of the isolated islets used for this study. The authors would also like to thank Pablo Garcia and Erika McCown for his technical assistance. We thank Dr. C.S. Jayasena (COH) for providing critical feedback and editing the manuscript.

Funding:
This work was supported by the National Institutes of Health (DK067912 and DK112917 to D.C.T, and DK102233 to D.C.T and R.V) and The Arthur Riggs Diabetes and Metabolism Research Institute (COH) Pilot program (R.V) and an American Heart Association Career Development Award to RB (25CDA1454374).

Duality of Interest. No potential conflicts of interest relevant to this article were reported.

Author Contributions
R.V conceptualized the project. D.C.T and R.V acquired the funding. J.H, K.E.M., M.A. R.V, and R.B performed the experiments and 2-DG uptake analysis. EO provided assistance with EndoC- βH5 cells culture. D.C.T, J.H. and R.V defined the methodology used. D.C.T supervised the project. R.V wrote the original draft of this manuscript. D.C.T, J.H. and R.V. were involved in the data analysis, discussion and editing of the manuscript. All authors approved the final version of the manuscript. R.V is the guarantor of this work and, as such, had full access to all the data in the study and takes responsibility for the integrity of the data and the accuracy of the data analysis.

References

1. Anonymous, International Diabetes Federation. *Diabetes Atlas* (2025).
2. K. Bouzakri *et al.*, Bimodal effect on pancreatic beta-cells of secretory products from normal or insulin-resistant human skeletal muscle. *Diabetes* **60**, 1111-1121 (2011).
3. S. Seino, T. Shibasaki, K. Minami, Dynamics of insulin secretion and the clinical implications for obesity and diabetes. *J Clin Invest* **121**, 2118-2125 (2011).
4. K. E. Merz, D. C. Thurmond, Role of Skeletal Muscle in Insulin Resistance and Glucose Uptake. *Compr Physiol* **10**, 785-809 (2020).
5. J. L. Jewell, E. Oh, D. C. Thurmond, Exocytosis mechanisms underlying insulin release and glucose uptake: conserved roles for Munc18c and syntaxin 4. *Am J Physiol Regul Integr Comp Physiol* **298**, R517-531 (2010).
6. M. A. Kalwat, S. M. Yoder, Z. Wang, D. C. Thurmond, A p21-activated kinase (PAK1) signaling cascade coordinately regulates F-actin remodeling and insulin granule exocytosis in pancreatic beta cells. *Biochem Pharmacol* **85**, 808-816 (2013).
7. K. E. Merz *et al.*, Changes in Skeletal Muscle PAK1 Levels Regulate Tissue Crosstalk to Impact Whole Body Glucose Homeostasis. *Front Endocrinol (Lausanne)* **13**, 821849 (2022).
8. L. Ramalingam, E. Oh, D. C. Thurmond, Doc2b enrichment enhances glucose homeostasis in mice via potentiation of insulin secretion and peripheral insulin sensitivity. *Diabetologia* **57**, 1476-1484 (2014).
9. T. Chattopadhyay, R. R. Singh, S. Gupta, A. Surolia, Bone morphogenetic protein-7 (BMP-7) augments insulin sensitivity in mice with type II diabetes mellitus by potentiating PI3K/AKT pathway. *Biofactors* **43**, 195-209 (2017).
10. D. Klein *et al.*, BMP-7 Induces Adult Human Pancreatic Exocrine-to-Endocrine Conversion. *Diabetes* **64**, 4123-4134 (2015).
11. H. Parikh *et al.*, TXNIP regulates peripheral glucose metabolism in humans. *PLoS Med* **4**, e158 (2007).
12. G. Xu, J. Chen, G. Jing, A. Shalev, Thioredoxin-interacting protein regulates insulin transcription through microRNA-204. *Nat Med* **19**, 1141-1146 (2013).
13. R. Veluthakal *et al.*, Restoration of Glucose-Stimulated Cdc42-Pak1 Activation and Insulin Secretion by a Selective Epac Activator in Type 2 Diabetic Human Islets. *Diabetes* **67**, 1999-2011 (2018).
14. R. Veluthakal, D. C. Thurmond, Emerging Roles of Small GTPases in Islet beta-Cell Function. *Cells* **10** (2021).
15. R. Veluthakal *et al.*, VAV2, a guanine nucleotide exchange factor for Rac1, regulates glucose-stimulated insulin secretion in pancreatic beta cells. *Diabetologia* **58**, 2573-2581 (2015).

16. Z. Wang, E. Oh, D. W. Clapp, J. Chernoff, D. C. Thurmond, Inhibition or ablation of p21-activated kinase (PAK1) disrupts glucose homeostatic mechanisms in vivo. *J Biol Chem* **286**, 41359-41367 (2011).
17. L. JeBailey *et al.*, Ceramide- and oxidant-induced insulin resistance involve loss of insulin-dependent Rac-activation and actin remodeling in muscle cells. *Diabetes* **56**, 394-403 (2007).
18. L. Sylow *et al.*, Rac1 governs exercise-stimulated glucose uptake in skeletal muscle through regulation of GLUT4 translocation in mice. *J Physiol* **594**, 4997-5008 (2016).
19. C. Dong, G. Wu, G-protein-coupled receptor interaction with small GTPases. *Methods Enzymol* **522**, 97-108 (2013).
20. V. O. Murovets, A. A. Bachmanov, V. A. Zolotarev, Impaired Glucose Metabolism in Mice Lacking the Tas1r3 Taste Receptor Gene. *PLoS One* **10**, e0130997 (2015).
21. I. Kojima, J. Medina, Y. Nakagawa, Role of the glucose-sensing receptor in insulin secretion. *Diabetes Obes Metab* **19 Suppl 1**, 54-62 (2017).
22. F. Wang *et al.*, The downregulation of sweet taste receptor signaling in enteroendocrine L-cells mediates 3-deoxyglucosone-induced attenuation of high glucose-stimulated GLP-1 secretion. *Arch Physiol Biochem* **124**, 430-435 (2018).
23. E. M. Wauson, E. Zaganjor, M. H. Cobb, Amino acid regulation of autophagy through the GPCR TAS1R1-TAS1R3. *Autophagy* **9**, 418-419 (2013).
24. H. E. Hohmeier *et al.*, Isolation of INS-1-derived cell lines with robust ATP-sensitive K+ channel-dependent and -independent glucose-stimulated insulin secretion. *Diabetes* **49**, 424-430 (2000).
25. P. Jiang *et al.*, Lactisole interacts with the transmembrane domains of human T1R3 to inhibit sweet taste. *J Biol Chem* **280**, 15238-15246 (2005).
26. J. Takasaki *et al.*, A novel Galphaq/11-selective inhibitor. *J Biol Chem* **279**, 47438-47445 (2004).
27. M. Ahn *et al.*, The p21-activated kinase (PAK1) is involved in diet-induced beta cell mass expansion and survival in mice and human islets. *Diabetologia* **59**, 2145-2155 (2016).
28. K. E. Merz *et al.*, Enrichment of the exocytosis protein STX4 in skeletal muscle remediates peripheral insulin resistance and alters mitochondrial dynamics via Drp1. *Nat Commun* **13**, 424 (2022).
29. R. Tunduguru *et al.*, Signaling of the p21-activated kinase (PAK1) coordinates insulin-stimulated actin remodeling and glucose uptake in skeletal muscle cells. *Biochem Pharmacol* **92**, 380-388 (2014).
30. R. Veluthakal, E. Oh, M. Ahn, D. Chatterjee Bhowmick, D. C. Thurmond, Syntaxin 4 Mediates NF-kappaB Signaling and Chemokine Ligand Expression via Specific Interaction With IkappaBbeta. *Diabetes* **70**, 889-902 (2021).
31. R. Balakrishnan *et al.*, Toward Ameliorating Insulin Resistance: Targeting a Novel PAK1 Signaling Pathway Required for Skeletal Muscle Mitochondrial Function. *Antioxidants (Basel)* **12** (2023).

32. R. Veluthakal, V. Sidarala, A. Kowluru, NSC23766, a Known Inhibitor of Tiam1-Rac1 Signaling Module, Prevents the Onset of Type 1 Diabetes in the NOD Mouse Model. *Cell Physiol Biochem* **39**, 760-767 (2016).
33. Y. C. Chen, A. J. Lutkewitte, H. D. Basavarajappa, P. T. Fueger, Glucolipotoxic Stress-Induced Mig6 Desensitizes EGFR Signaling and Promotes Pancreatic Beta Cell Death. *Metabolites* **13** (2023).
34. S. K. Sukumaran, S. R. Palayyan, Sweet Taste Signaling: The Core Pathways and Regulatory Mechanisms. *Int J Mol Sci* **23** (2022).
35. R. Ahmad, J. E. Dalziel, G Protein-Coupled Receptors in Taste Physiology and Pharmacology. *Front Pharmacol* **11**, 587664 (2020).
36. A. Sassmann *et al.*, The Gq/G11-mediated signaling pathway is critical for autocrine potentiation of insulin secretion in mice. *J Clin Invest* **120**, 2184-2193 (2010).
37. A. Keech *et al.*, Effects of long-term fenofibrate therapy on cardiovascular events in 9795 people with type 2 diabetes mellitus (the FIELD study): randomised controlled trial. *Lancet* **366**, 1849-1861 (2005).
38. S. N. Liu *et al.*, Long-term fenofibrate treatment impaired glucose-stimulated insulin secretion and up-regulated pancreatic NF-kappa B and iNOS expression in monosodium glutamate-induced obese rats: is that a latent disadvantage? *J Transl Med* **9**, 176 (2011).
39. J. A. Balfour, D. McTavish, R. C. Heel, Fenofibrate. A review of its pharmacodynamic and pharmacokinetic properties and therapeutic use in dyslipidaemia. *Drugs* **40**, 260-290 (1990).
40. S. M. Yoder, S. L. Dineen, Z. Wang, D. C. Thurmond, YES, a Src family kinase, is a proximal glucose-specific activator of cell division cycle control protein 42 (Cdc42) in pancreatic islet beta cells. *J Biol Chem* **289**, 11476-11487 (2014).
41. N. J. Pavlos, P. A. Friedman, GPCR Signaling and Trafficking: The Long and Short of It. *Trends Endocrinol Metab* **28**, 213-226 (2017).
42. B. Jones *et al.*, Targeting GLP-1 receptor trafficking to improve agonist efficacy. *Nat Commun* **9**, 1602 (2018).
43. R. A. DeFronzo, D. Tripathy, Skeletal muscle insulin resistance is the primary defect in type 2 diabetes. *Diabetes Care* **32 Suppl 2**, S157-163 (2009).
44. R. Tunduguru *et al.*, The actin-related p41ARC subunit contributes to p21-activated kinase-1 (PAK1)-mediated glucose uptake into skeletal muscle cells. *J Biol Chem* **292**, 19034-19043 (2017).
45. P. Han, R. Keast, E. Roura, TAS1R1 and TAS1R3 Polymorphisms Relate to Energy and Protein-Rich Food Choices from a Buffet Meal Respectively. *Nutrients* **10** (2018).
46. P. Huang, Y. M. Altshuller, J. C. Hou, J. E. Pessin, M. A. Frohman, Insulin-stimulated plasma membrane fusion of Glut4 glucose transporter-containing vesicles is regulated by phospholipase D1. *Mol Biol Cell* **16**, 2614-2623 (2005).
47. R. Tunduguru, D. C. Thurmond, Promoting Glucose Transporter-4 Vesicle Trafficking along Cytoskeletal Tracks: PAK-Ing Them Out. *Front Endocrinol (Lausanne)* **8**, 329 (2017).

48. M. A. Kalwat, D. C. Thurmond, Signaling mechanisms of glucose-induced F-actin remodeling in pancreatic islet beta cells. *Exp Mol Med* **45**, e37 (2013).
49. Y. M. Ikushima *et al.*, MEK/ERK Signaling in beta-Cells Bifunctionally Regulates beta-Cell Mass and Glucose-Stimulated Insulin Secretion Response to Maintain Glucose Homeostasis. *Diabetes* **70**, 1519-1535 (2021).
50. S. K. Ramakrishnan *et al.*, Fenofibrate Decreases Insulin Clearance and Insulin Secretion to Maintain Insulin Sensitivity. *J Biol Chem* **291**, 23915-23924 (2016).
51. M. Kochem, P. A. Breslin, Lipid-Lowering Pharmaceutical Clofibrate Inhibits Human Sweet Taste. *Chem Senses* **42**, 79-83 (2017).
52. Y. C. Ma, J. Huang, S. Ali, W. Lowry, X. Y. Huang, Src tyrosine kinase is a novel direct effector of G proteins. *Cell* **102**, 635-646 (2000).
53. D. B. J. Bone *et al.*, Skeletal Muscle-Specific Activation of G(q) Signaling Maintains Glucose Homeostasis. *Diabetes* **68**, 1341-1352 (2019).

Figure Legends

Figure 1. TAS1R3 expression is significantly lower in human islets from T2D individuals compared to non-diabetic individuals.

(**A**) Densitometry analysis of TAS1R3 protein abundance in human T2D (n=3 donors) versus non-diabetic (ND; n=4 donors) islets. Top: Representative immunoblot (IB). Vertical dashed line indicates splicing of lanes from within the same gel exposure. Control: tubulin (Tub). (**B**) Quantification of TAS1R3 mRNA expression relative to tubulin mRNA expression in human T2D (n=6 donors) versus ND (n=7 donors) islets by qPCR. (**C-D**) INS-1 832/13 cells were untreated (0 h) or exposed to glucolipotoxic (GLT) stress (0.4 mM palmitate and 25 mM high glucose) for up to 24 h (n=5 independent experiments). (**C**) Densitometry TAS1R3 protein abundance relative to tubulin protein levels. Top: Representative IB. CHOP indicates ER stress-induction with GLT-treatment. (**D**) Quantification of TAS1R3 mRNA (normalized to tubulin) by qPCR. TAS1R3 mRNA at 0 h (fold-change set to 1.0) compared to 16 h and 24 h exposure . (A-D) Data expressed as mean ± SEM; N.S., not significant. *$p < 0.05$, **$p < 0.01$, ***$p < 0.001$. ****$p < 0.0001$.

Figure 2. Lactisole and fenofibrate inhibit GSIS from human islets and human EndoC- βH5 cells.

Human islets (**A**, n=6 islet donors) and EndoC-βH5 (**B**, 4-7 independent experiments) were incubated with TAS1R3 inhibitor (lactisole, 1 mM) or Gαq/11 inhibitor (YM-25490, 10 μM) to test their abilities to alter GSIS. Vehicle: DMSO. The indicated compounds were added for 20 min prior to stimulatory glucose exposure (20 mM for 1 h in (**A**) or

16.7 mM for 45 min in (**B**). Secreted insulin values were normalized to the insulin content. (**C**) EndoC-βH5 cells were pre-incubated with test compounds for 20 min, and then exposed to stimulatory glucose (16.7 mM) for 45 min (n=5 independent experiments). cAMP levels were quantified and normalized to total protein. (**D**) Effect of cholesterol drug and TAS1R3 inhibitor, fenofibrate (10 and 27.17 μM) on INS-1 832/13 cell GSIS. Fenofibrate was added 20 min pre-stimulatory glucose (20 mM) exposure. N=6 independent experiments. Secreted insulin values were normalized to total cellular protein content. (A-D) Data expressed as mean ± SEM; N.S., not significant. *$p < 0.05$, **$p < 0.01$, ***$p < 0.001$. ****$p < 0.0001$.

Figure 3. TAS1R3 knockdown attenuates GSIS from rat INS-1 832/13 cells.

(**A**) Impact of TAS1R3 knockdown with small interfering RNA (siRNA) on TAS1R3 protein abundance in INS-1 832/13 cells. Top: Representative immunoblot (IB). Bottom: densitometry analysis of TAS1R3 protein expression normalized to tubulin from siRNA treated cells (n=4 independent experiments). TAS1R3 abundance from non-transfected cells was set to 1.0. (**B**) Impact of TAS1R3 siRNA knockdown on GSIS in INS-1 832/13 cells. Post-siRNA treatment, cells were exposed to glucose (20 mM) for 45 min (n= 5 independent experiments). Secreted insulin values were normalized to total cellular protein content. (**A-B**) Data expressed as mean ± SEM; N.S., not significant.** $p < 0.01$ and **** $p < 0.0001$.

Figure 4. Lactisole inhibits, while YM-25490 fails to inhibit phospho-SFK and Cdc42 activation in EndoC-βH1cells and human islets, attenuates plasma membrane -localized TAS1R3 abundance

EndoC-βH1 cells (**A, C**) and human islets (**B**) were treated with TAS1R3*i* lactisole (1 mM) or Gαq/11*i* YM-25490 (10 μM) for 20 min. Following this, cells were exposed to glucose (2.8 mM or 16.7 mM) for 1 min for phospho-SFK (p-SFK) activation (**A**) and 2 min for Cdc42 activation (**B, C**). (**A**) Densitometry analysis of p-SFK normalized to t-SFK (n=5 independent experiments). Top: Representative immunoblot (IB). (**B-C**) Cdc42-GTP was detected by G-LISA (n=5 donors in (**B**) and n=4 independent experiments in (**C**). Values are relative to baseline Cdc42-GTP levels detected with 2.8 mM glucose stimulation.

(**D**) Plasma membrane fractions were isolated from 2.8 mM and 16.7 mM glucose-stimulated **EndoC-**βH1cells and treated with TAS1R3*i* lactisole (15 min). Top: representative immunoblot (IB). Rho-GDI, a cytosolic marker, demonstrates purity of the PM fractions. For densitometry analysis, abundance of TAS1R3 were normalized relative to syntaxin 4 (STX4) levels (n=4 independent experiment). WCL: whole cell lysates. Data expressed as mean ± SEM; N.S., not significant. **p < 0.01, ***p < 0.001. ****p < 0.0001.

Figure 5. TAS1R3 abundance is lower in skeletal muscle from T2D individuals compared to non-diabetic individuals.

(**A**). LHCN-M2 myotube cells were untreated or exposed to glucolipotoxic (GLT) stress for up to 24 h (n=6 independent experiments). TAS1R3 mRNA was expressed as relative to tubulin mRNA. (**B**) Quantification of TAS1R3 mRNA expression in skeletal muscle from T2D (n=6 donors) versus non-diabetic (ND, n=6 donors) individuals using qPCR. TAS1R3 mRNA was expressed as relative to tubulin mRNA. (**C**) Densitometry analysis of TAS1R3 protein in skeletal muscle from T2D (n=5 donors) versus ND (n=6 donors) individuals. Top: representative immunoblot (IB). TAS1R3 protein was expressed as relative to GAPDH.

Vertical dashed lines indicate splicing of lanes from within the same gel exposure. **(A-C**). Data expressed as mean ± SEM. *p < 0.05, **p < 0.01.

Figure 6. Lactisole inhibits insulin-stimulated glucose uptake and Rac1 activation in human LHCN-M2 myotubes.

Assessment of 2-deoxyglucose uptake ([^{3}H]2-DG) uptake (20 min) (**A**) and Rac1 activation (10 min) (**B**) in LHCN-M2 myotubes. Myotubes were pre-treated with TAS1R3 inhibitor lactisole or Gαq/11 inhibitor YM-25490 for 20 min and then stimulated with insulin. (**A**) Glucose uptake was normalized to protein content. Cpm: Counts per minute (n=4 independent experiments). (**B**) Rac1 activation values are relative to baseline Rac1-GTP levels (set to 1.0) detected with unstimulated basal insulin (n=5 independent experiments). **(C-D)** Impact of TAS1R3 knockdown with small interfering RNA (siRNA) in human LHCN-M2 myotube cells. (**C**) Top: Representative immunoblot (IB). Bottom: Densitometry analysis of TAS1R3 protein expression normalized to tubulin (Tub). Control-siRNA values were set to 1.0. N=4 independent experiments. (**D**) Effects of siRNA treatment on glucose uptake with insulin stimulation (n= 8 independent experinments) Glucose uptake was normalized to protein content. Cpm: Counts per minute . Values under basal unstimulated insulin conditions were set to 1.0. (**A-D**) Data expressed as mean ± SEM. * p < 0.05, ** p < 0.01, *** p < 0.001 and **** p < 0.0001. N.S: not significant.

Figure 7. Lactisole fails to inhibit the activation of IRS and AKT but prevents the dephosphorylation of cofilin.

(A-C) LHCN-M2 myotubes were pre-treated with vehicle (DMSO), TAS1R3*i* r lactisole or Gαq/11*i* YM-25490 for 1 h and were stimulated with ± 100 nM insulin (10 min). A representative immunoblot and densitometry analysis is shown for phospho-IRS (Tyr^{608}) and total IRS (**A**) (n=4 independent experiments), phospho-AKT (Ser^{473}) and total AKT (**B**) (n=5 independent experiments), and phospho-cofilin (Ser^{3}) and total cofilin (**C**) (n=5 independent experiments). Data expressed as mean ± SEM. * $p < 0.05$, ** $p < 0.01$, *** $p < 0.001$ and **** $p < 0.0001$. N.S: not significant.

Figure 1

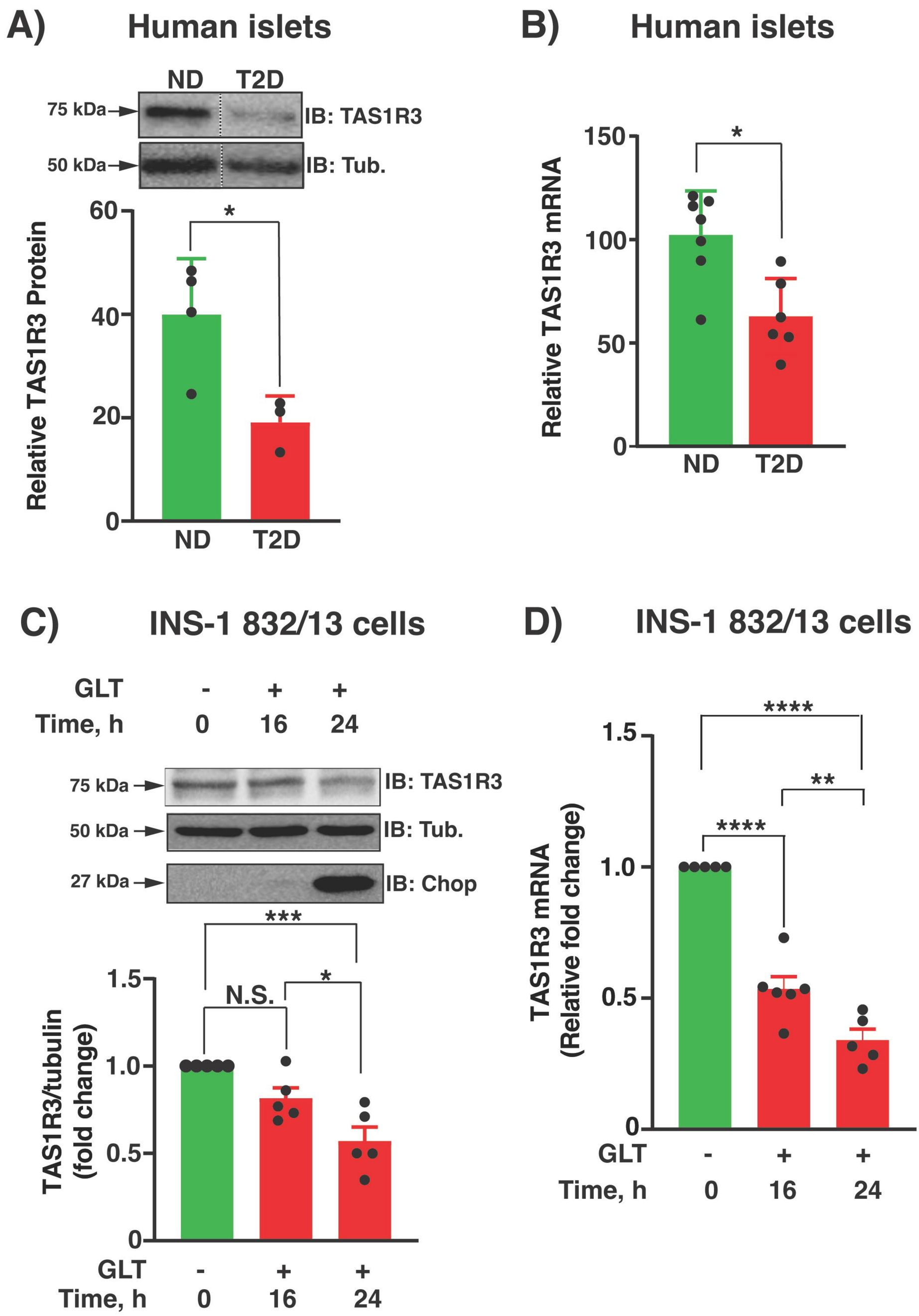
A)
Human islets
ND
T2D
75 kDa
IB: TAS1R3
50 kDa
IB: Tub.
Relative TAS1R3 Protein
60
40
20
0
*
ND
T2D
B)
Human islets
Relative TAS1R3 mRNA
150
100
50
0
*
ND
T2D
C)
INS-1 832/13 cells
GLT - + +
Time, h 0 16 24
75 kDa
IB: TAS1R3
50 kDa
IB: Tub.
27 kDa
IB: Chop
TAS1R3/tubulin (fold change)
1.5
1.0
0.5
0
***
N.S.
*
GLT - + +
Time, h 0 16 24
D)
INS-1 832/13 cells
TAS1R3 mRNA (Relative fold change)
1.5
1.0
0.5
0
****
**
****
GLT - + +
Time, h 0 16 24

Figure 2

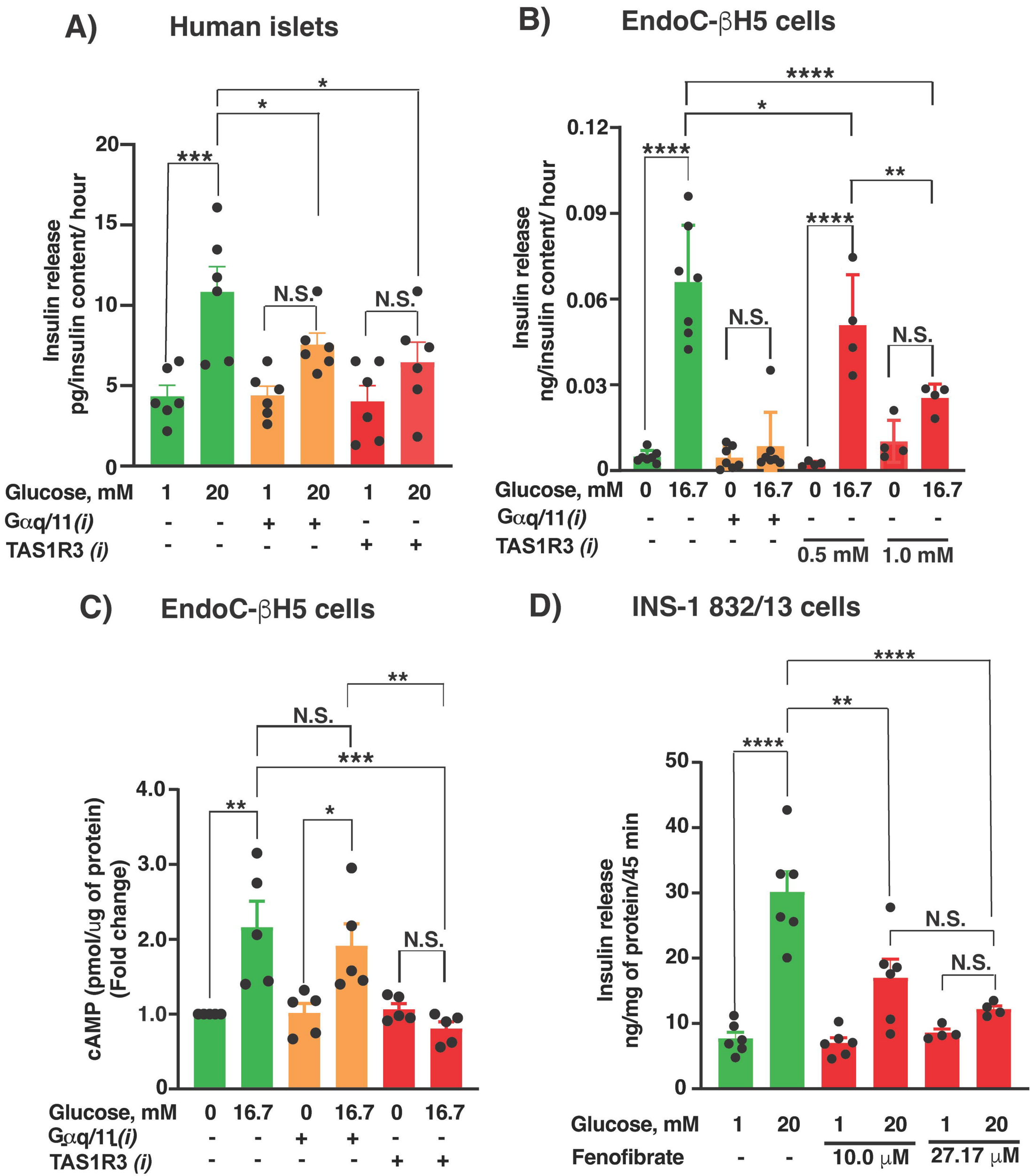
A)
Human islets
Insulin release
pg/insulin content/ hour
20
15
10
5
0
***
*
*
N.S.
N.S.
Glucose, mM 1 20 1 20 1 20
Gαq/11 (i) - - + + - -
TAS1R3 (i) - - - - + +
B)
EndoC-βH5 cells
Insulin release
ng/insulin content/ hour
0.12
0.09
0.06
0.03
0
****
*
****
**
****
N.S.
N.S.
Glucose, mM 0 16.7 0 16.7 0 16.7 0 16.7
Gαq/11 (i) - - + + - - - -
TAS1R3 (i) - - - - 0.5 mM 1.0 mM
C)
EndoC-βH5 cells
cAMP (pmol/ug of protein)
(Fold change)
4.0
3.0
2.0
1.0
0
**
N.S.
***
**
*
N.S.
Glucose, mM 0 16.7 0 16.7 0 16.7
Gαq/11 (i) - - + + - -
TAS1R3 (i) - - - - + +
D)
INS-1 832/13 cells
Insulin release
ng/mg of protein/45 min
50
40
30
20
10
0
****
**
****
****
N.S.
N.S.
Glucose, mM 1 20 1 20 1 20
Fenofibrate - - 10.0 μM 27.17 μM

Figure 3

A) INS-1 832/13 cells

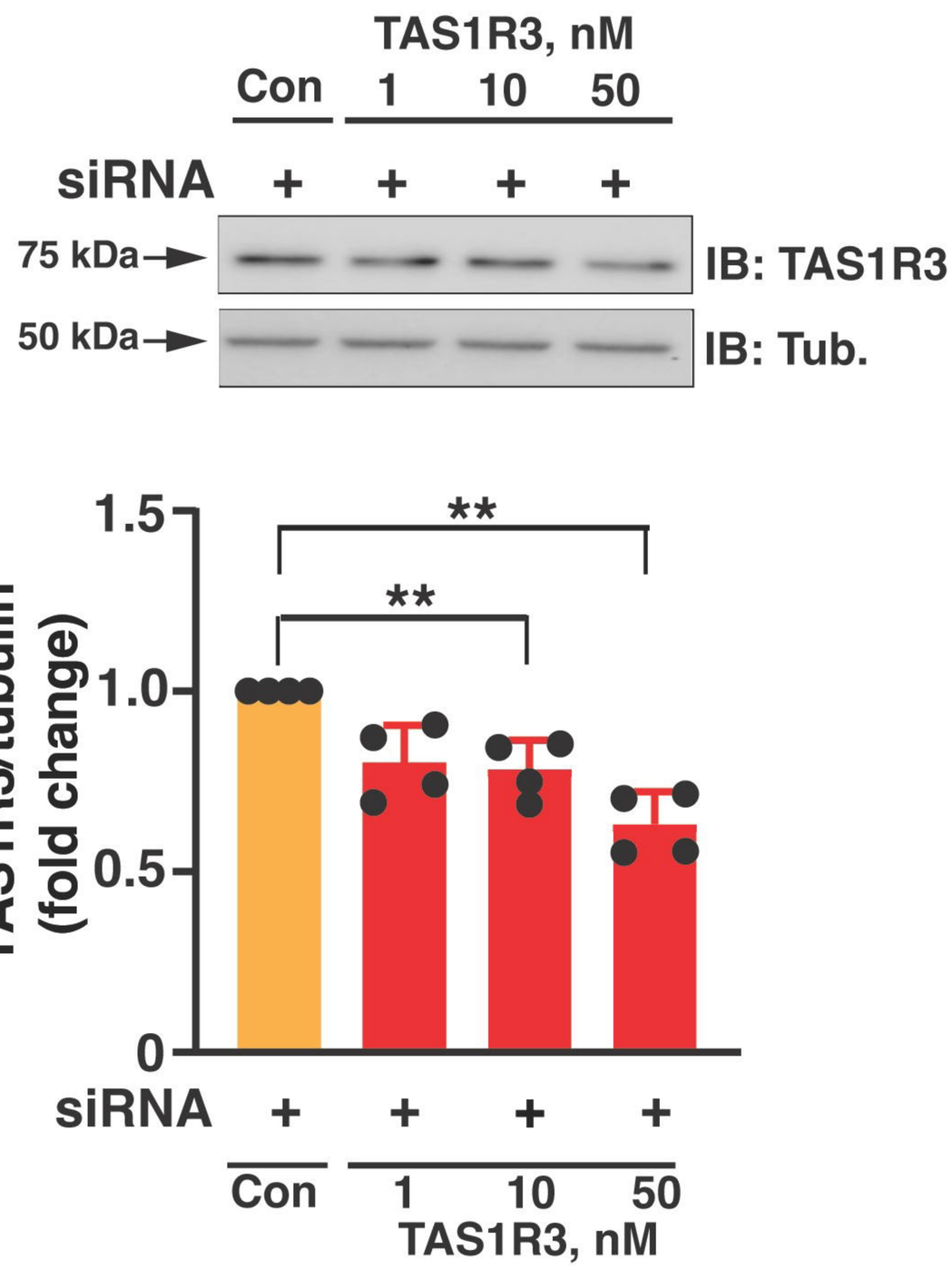

B) INS-1 832/13 cells

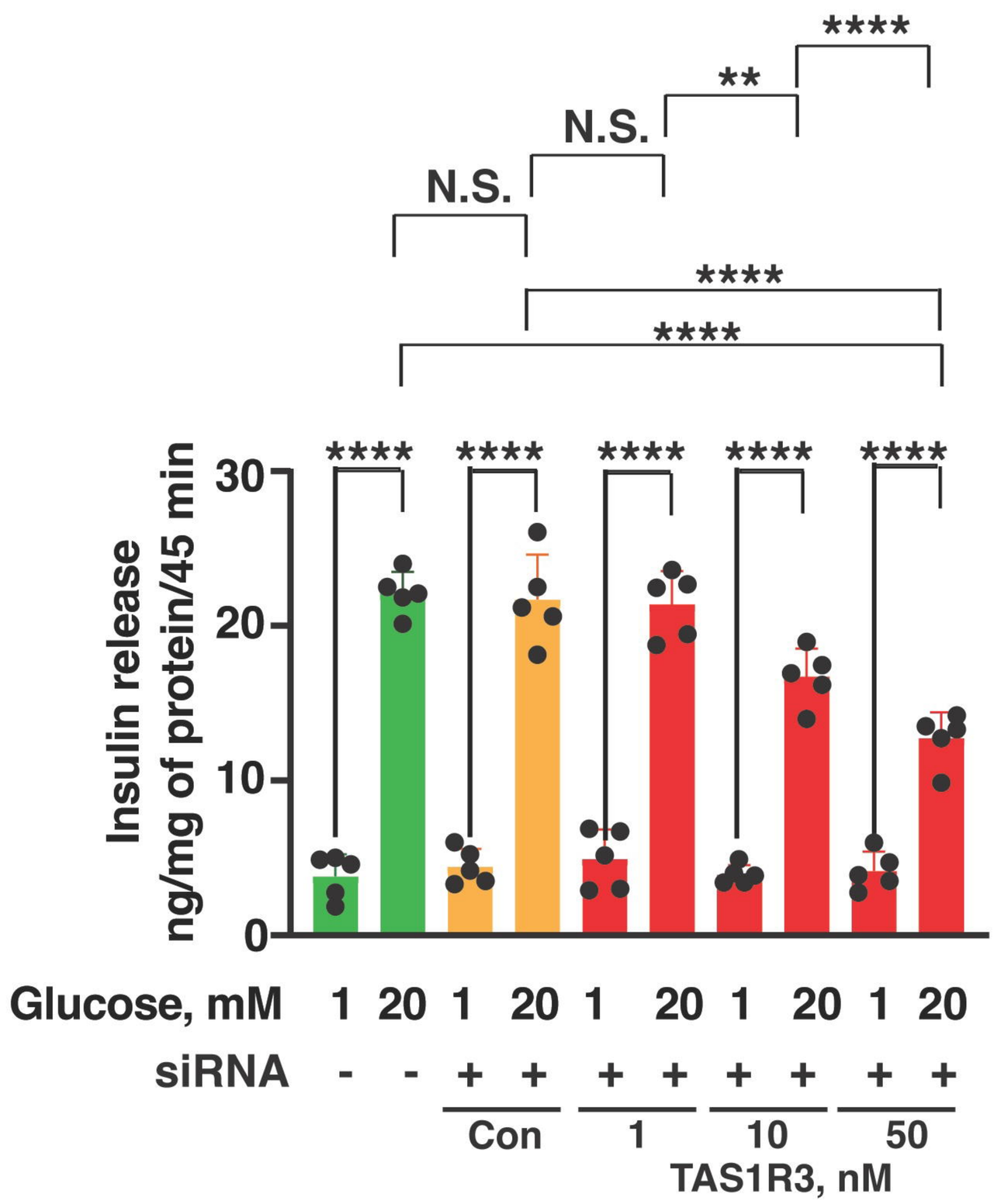

Figure 4

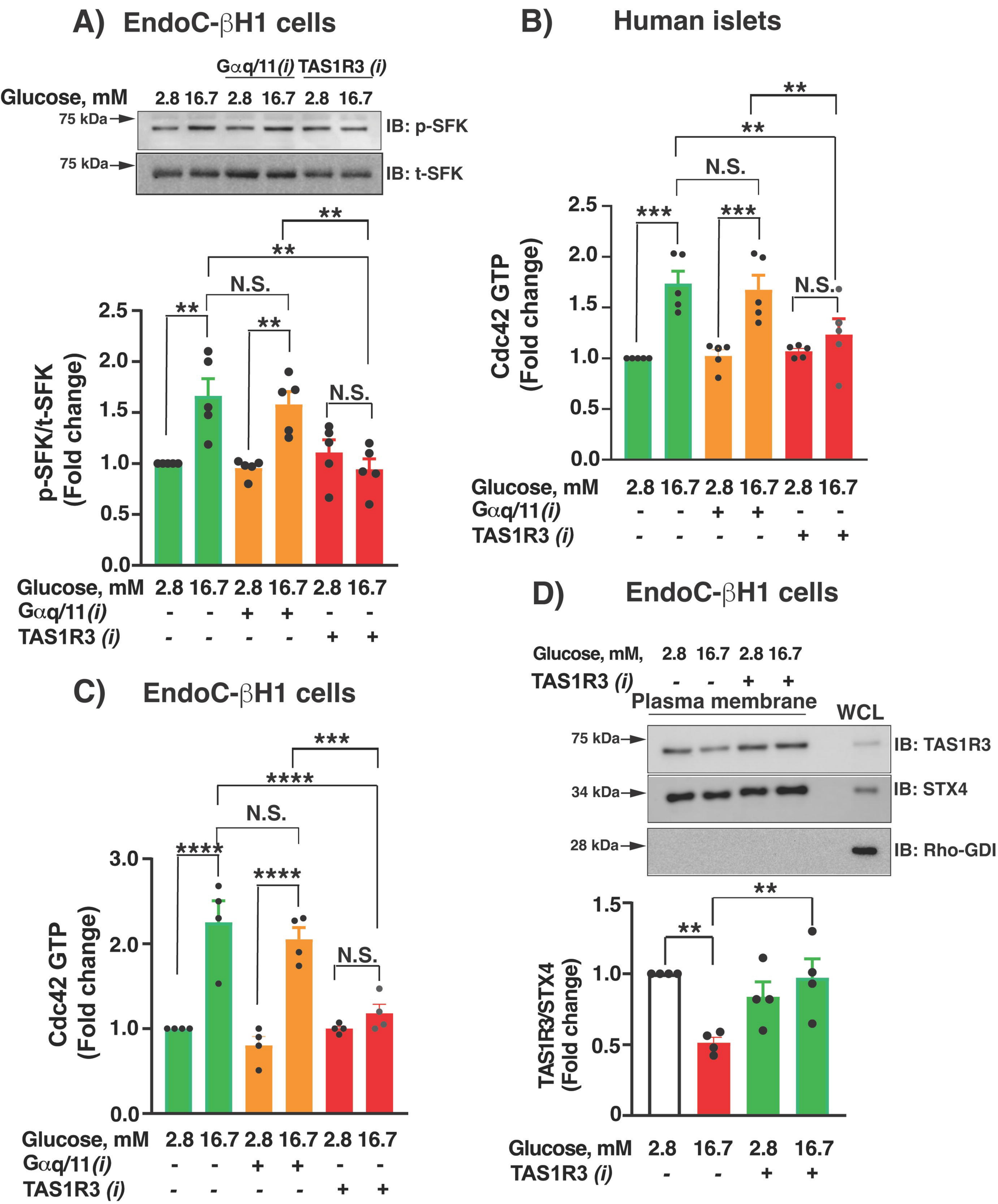
A) EndoC-βH1 cells
Gαq/11 (i)
TAS1R3 (i)
Glucose, mM 2.8 16.7 2.8 16.7 2.8 16.7
75 kDa
IB: p-SFK
75 kDa
IB: t-SFK
p-SFK/t-SFK (Fold change)
2.5
2.0
1.5
1.0
0.5
0.0
**
**
N.S.
**
**
N.S.
Glucose, mM 2.8 16.7 2.8 16.7 2.8 16.7
Gαq/11 (i) - - + + - -
TAS1R3 (i) - - - - + +
B) Human islets
Cdc42 GTP (Fold change)
2.5
2.0
1.5
1.0
0.5
0.0
**
**
N.S.
***
***
N.S.
Glucose, mM 2.8 16.7 2.8 16.7 2.8 16.7
Gαq/11 (i) - - + + - -
TAS1R3 (i) - - - - + +
C) EndoC-βH1 cells
Cdc42 GTP (Fold change)
3.0
2.0
1.0
0.0
***
****
N.S.
****
****
N.S.
Glucose, mM 2.8 16.7 2.8 16.7 2.8 16.7
Gαq/11 (i) - - + + - -
TAS1R3 (i) - - - - + +
D) EndoC-βH1 cells
Glucose, mM, 2.8 16.7 2.8 16.7
TAS1R3 (i) - - + +
Plasma membrane
WCL
75 kDa
IB: TAS1R3
34 kDa
IB: STX4
28 kDa
IB: Rho-GDI
TAS1R3/STX4 (Fold change)
1.5
1.0
0.5
0
**
**
Glucose, mM 2.8 16.7 2.8 16.7
TAS1R3 (i) - - + +

Figure 5

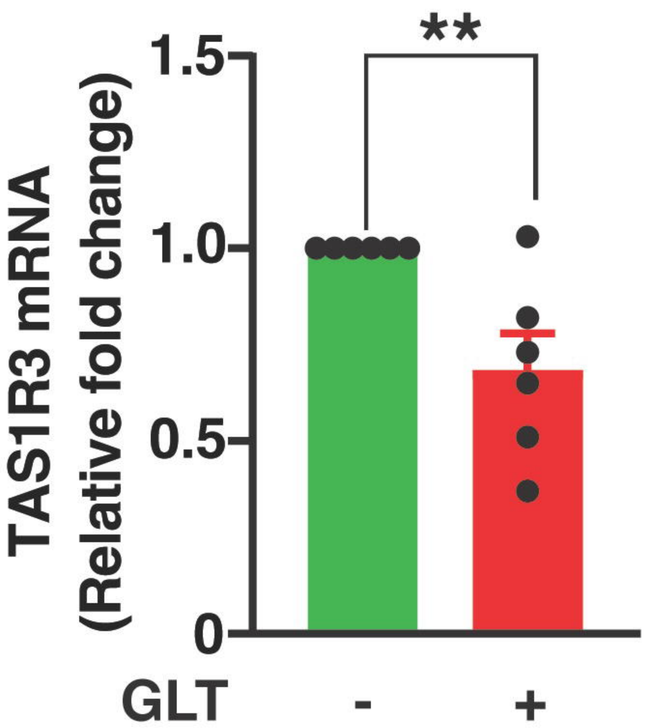
A) Human LHCN-M2 cells
**
TAS1R3 mRNA
(Relative fold change)
1.5
1.0
0.5
0
GLT
-
+

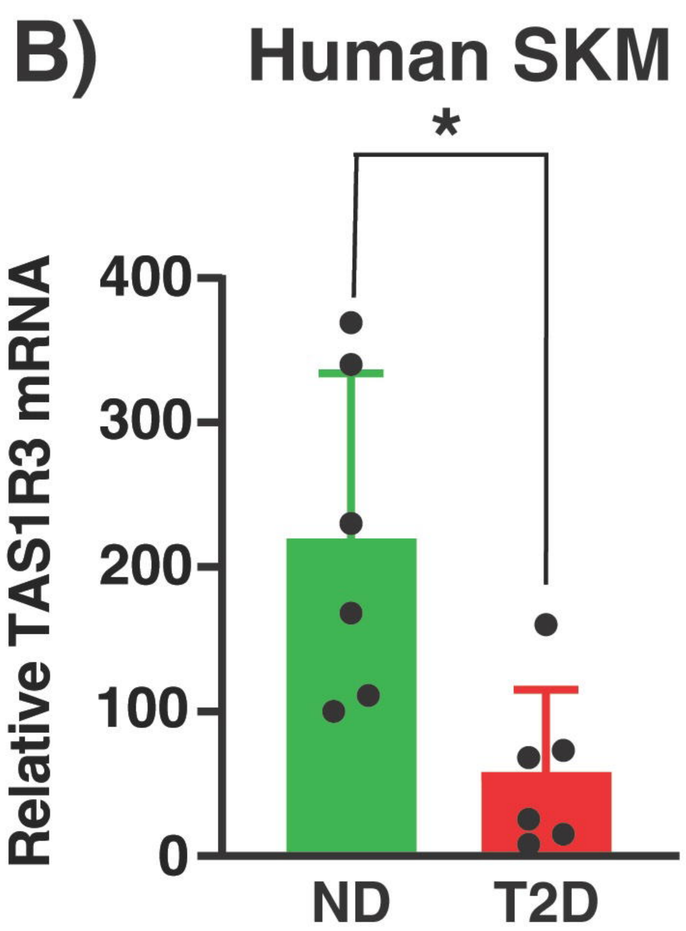
B) Human SKM
*
Relative TAS1R3 mRNA
400
300
200
100
0
ND
T2D

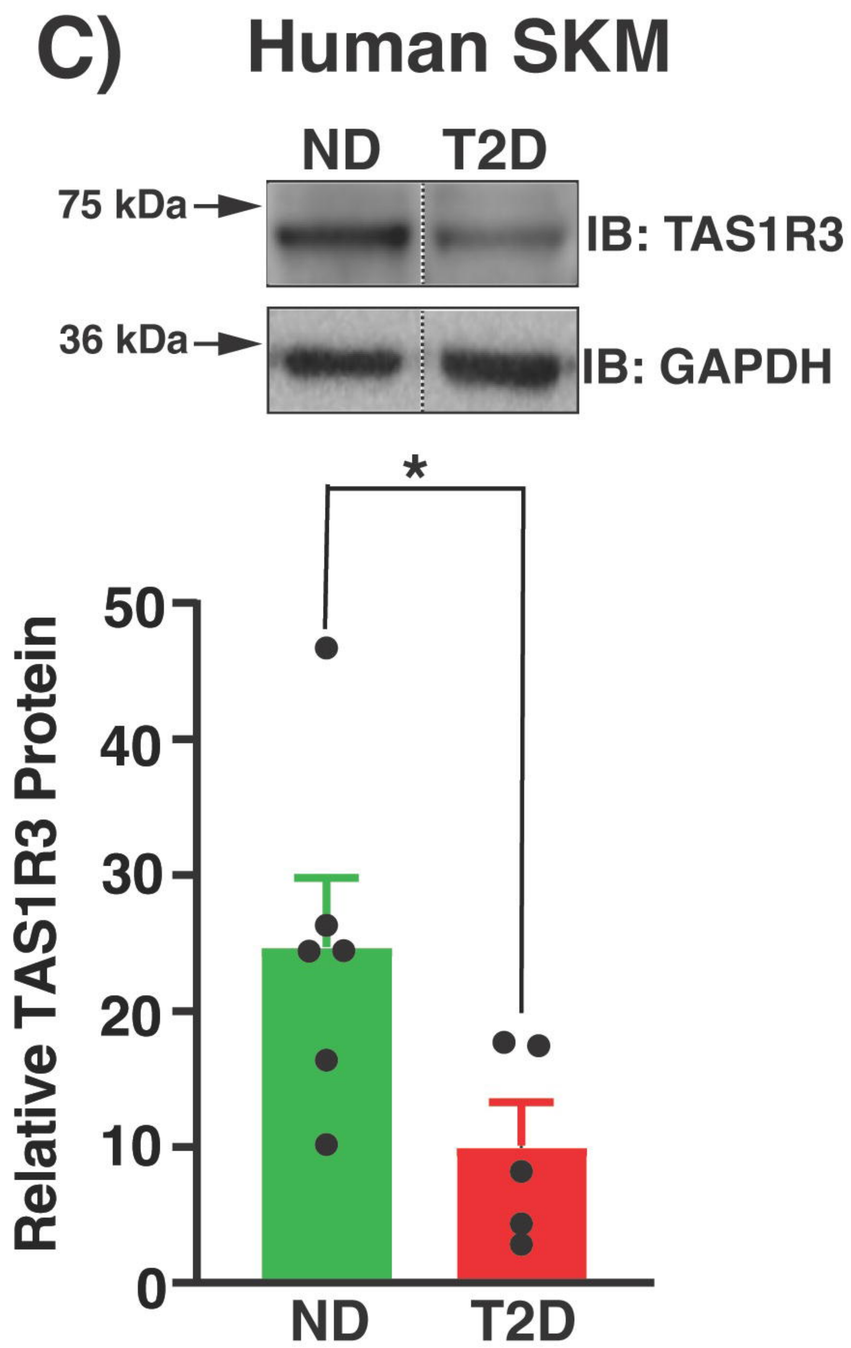
C) Human SKM
ND
T2D
75 kDa
IB: TAS1R3
36 kDa
IB: GAPDH
*
Relative TAS1R3 Protein
50
40
30
20
10
0
ND
T2D

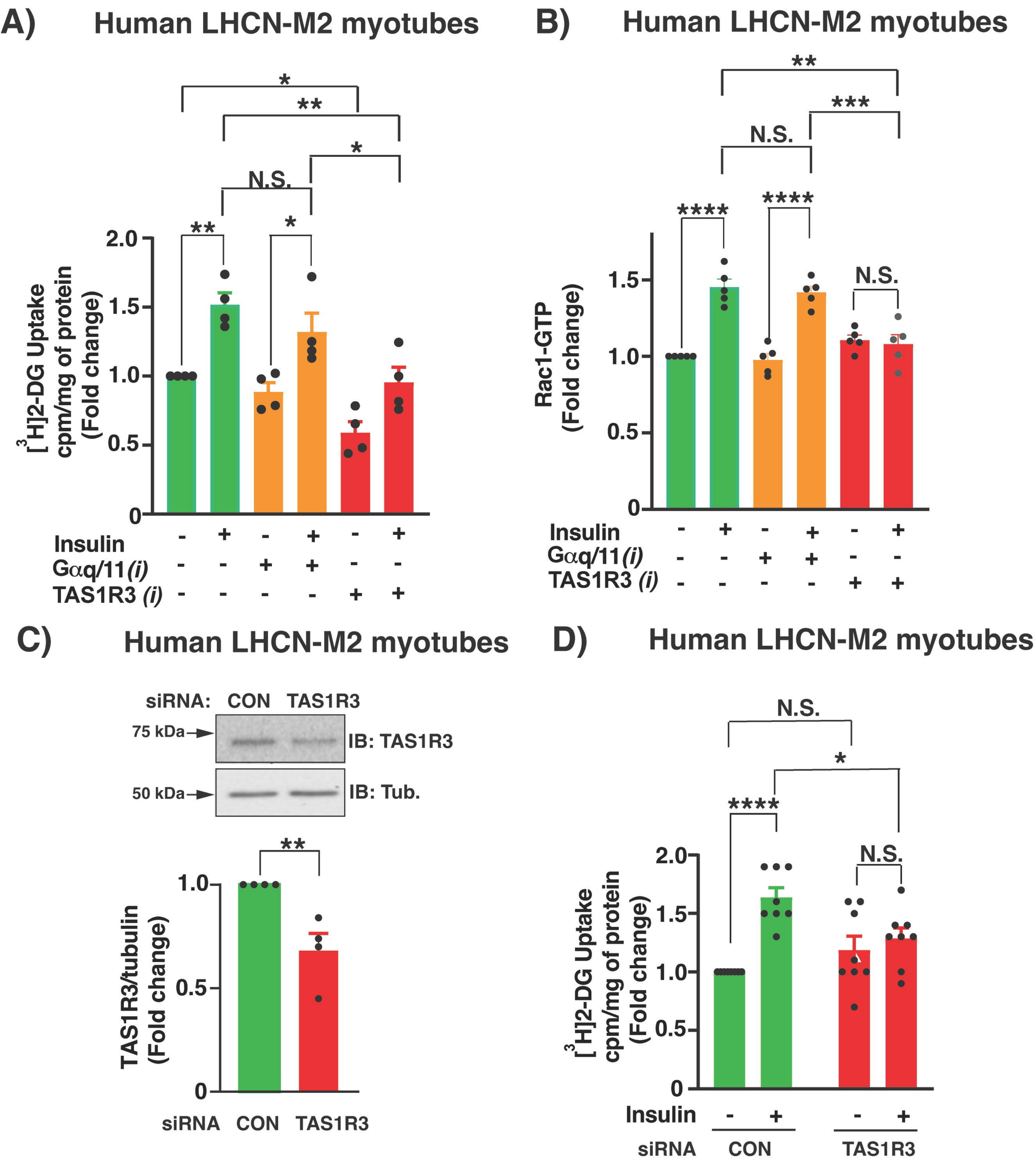
A)
Human LHCN-M2 myotubes
[3H]2-DG Uptake cpm/mg of protein (Fold change)
2.0
1.5
1.0
0.5
0
*
**
*
N.S.
**
*
Insulin - + - + - +
Gαq/11 (i) - - + + - -
TAS1R3 (i) - - - - + +
B)
Human LHCN-M2 myotubes
Rac1-GTP (Fold change)
1.5
1.0
0.5
0
**
***
N.S.
****
****
N.S.
Insulin - + - + - +
Gαq/11 (i) - - + + - -
TAS1R3 (i) - - - - + +
C)
Human LHCN-M2 myotubes
siRNA: CON TAS1R3
75 kDa
IB: TAS1R3
50 kDa
IB: Tub.
TAS1R3/tubulin (Fold change)
1.0
0.5
0
**
siRNA CON TAS1R3
D)
Human LHCN-M2 myotubes
[3H]2-DG Uptake cpm/mg of protein (Fold change)
2.0
1.5
1.0
0.5
0
N.S.
*
****
N.S.
Insulin - + - +
siRNA CON TAS1R3

Figure 7

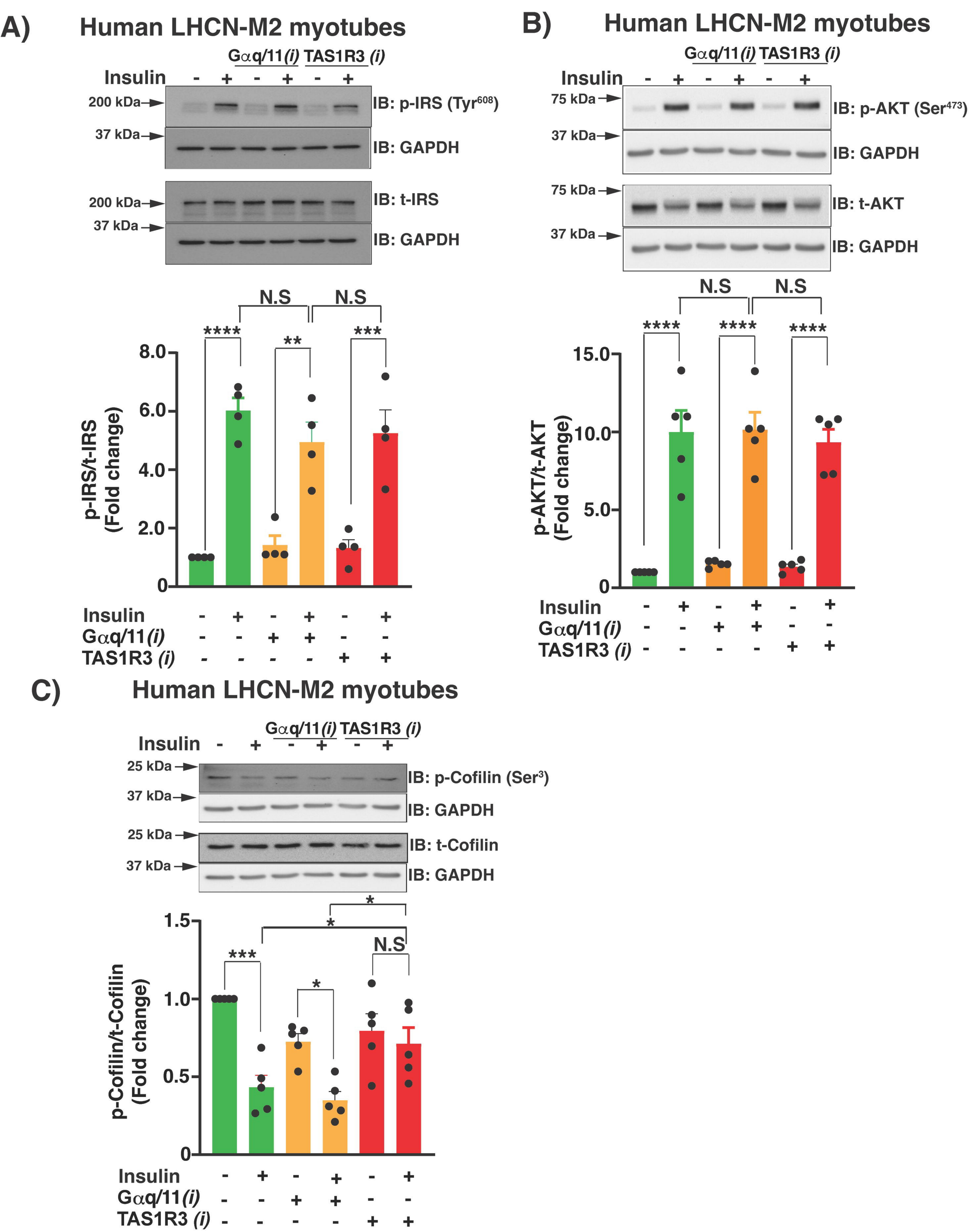
A)
Human LHCN-M2 myotubes
Gαq/11 (i)
TAS1R3 (i)
Insulin
200 kDa
37 kDa
IB: p-IRS (Tyr608)
IB: GAPDH
IB: t-IRS
IB: GAPDH
N.S
N.S
****
**
***
p-IRS/t-IRS (Fold change)
8.0
6.0
4.0
2.0
0
Insulin
Gαq/11 (i)
TAS1R3 (i)
B)
Human LHCN-M2 myotubes
75 kDa
37 kDa
IB: p-AKT (Ser473)
IB: GAPDH
IB: t-AKT
IB: GAPDH
N.S
N.S
****
****
****
p-AKT/t-AKT (Fold change)
15.0
10.0
5.0
0
C)
Human LHCN-M2 myotubes
25 kDa
37 kDa
IB: p-Cofilin (Ser3)
IB: GAPDH
IB: t-Cofilin
IB: GAPDH
*
*
N.S
***
*
p-Cofilin/t-Cofilin (Fold change)
1.5
1.0
0.5
0